Investigation of focused ion beam induced damage in single crystal diamond tools

Zhen Tong[1,2], Xichun Luo[1*]

1 Centre for Precision Manufacturing, Department of Design, Manufacture & Engineering Management, University of Strathclyde, Glasgow G1 1XQ, UK

2 Center for Precision Engineering, Harbin Institute of Technology, Harbin 150001, China

**Email: Xichun.Luo@strath.ac.uk*

Abstract

In this work, transmission electron microscope (TEM) measurements and molecular dynamic (MD) simulations were carried out to characterise the focused ion beam (FIB) induced damage layer in a single crystal diamond tool under different FIB processing voltages. The results obtained from the experiments and the simulations are in good agreement. The results indicate that during the FIB processing cutting tools made of natural single crystal diamond, the energetic Ga^+ collision will create an impulse-dependent damage layer at the irradiated surface. For the tested beam voltages in a typical FIB system (from 8 kV to 30 kV), the thicknesses of the damaged layers formed on a diamond tool surface increased from 11.5 nm to 27.6 nm. The dynamic damage process of FIB irradiation and ion-solid interactions physics leading to processing defects in FIB milling were emulated by MD simulations. The research findings from this study provide the in-depth understanding of the wear of nanoscale multi-tip diamond tools considering the FIB irradiation induced doping and defects during the tool fabrication process.

(Some figures in this article are in colour only in the electronic version)

Keywords: molecular dynamics; focused ion beam; irradiation damage; amorphization; diamond tool.

1 Introduction

In recent decades, single point diamond turning and milling using micro tools as well as their extensions have been widely used in the fabrication of periodic micro-structures in various materials [1-4]. However, the size and configuration limitations of the cutting tools limit the diamond machining to create patterns of sub-micro/nanostructures, especially high aspect ratio structures. Focused ion beam (FIB) machining technique has been developed up-to-date as an indispensable tool to effectively shape micro- and nanoscale diamond tools by sputtering diamond tool tip with nanometre precision [5-9]. With the advance of controlled FIB processing of micro diamond tools, varieties of tool geometries such as single tipped and dual-tipped tools having rectangular, triangular, and other complex shaped face designs have been produced to generate functional structured surface through ultra-precision diamond turning [7, 10-12]. This approach therefore, fully utilises the fine process capability of the physical sputtering actions of FIB and the high productivity of diamond turning. Most recently, nano-gratings with the pitch as small as hundreds of nanometres can also be generated by this technique using nanoscale multi-tip diamond tools [13, 14].

Despite these breakthroughs, the exposure of a diamond tool to FIB will result in the implantation of ion source material and the irradiation damage of the milled area at the near surface. This modification would alternate the surface composition and cause surface instability [15, 16]. For the application of micro- and nanoscale diamond tools, the ion irradiation induced doping and defects will unavoidably degrade the cutting performance of the diamond tools fabricated by FIB. Therefore, the characterization of ion-induced damage layer and the in-depth understanding of the ion-solid interactions physics leading to processing defects in FIB machining are significant to develop an effective way to control and minimise the formation of residual damage on micro- and nanoscale diamond tool tips.

In recent years, a variety of experimental techniques including Raman spectroscopy [17], transmission electron microscope (TEM) [18, 19], and secondary ion mass spectrometry (SIMS) [16] have been used to study the ion-induced damage in diamond. Admas *et al*. [9] used TEM to study the amorphous carbon layer in single crystal diamond tool created by FIB milling and a larger amorphous layer was

found when a small local incident angle of ion beam applied. Rubanov *et al*. [18] investigated the ion-induced damage layers in a synthetic type1b diamond substrate under eight different ion doses. The thickness of the damage layer grew with the ion dose and achieved an equilibrium value of 44 nm for continuous 30 keV Ga^+ FIB milling [18]. Mckenzie *et al*. [19] reported that the near surface microstructure of a single crystal natural conductive diamond varies with the increase of ion dose, and the critical dose for the amorphization of the diamond substrate (thickness of 35 nm) is 2.0×10^{14} ions/cm^2. Additionally, Gnaser and co-workers [16] has reported a fluence-dependent evolution of the implanted Ga concentration in nanocrystalline diamond films by SIMS. These experiments demonstrate the existence of FIB-induced damage layer in different kinds of diamond materials. However, most of the experimental works were concentrated on the CVD or doped conductive diamond. Little work has been found to characterise the FIB-induced damage on natural single crystal diamond used in cutting tools. This might be due to the difficulties involved in fabricating large, flat and uniform TEM samples in undoped non-conductive diamond. The beam drift caused by electrostatic charging has to be resolved. Moreover, only the ion dose is measurable in a typical FIB irradiation and TEM experiment. The post-facto-observation leaves a gap in understanding the whole picture of damage evolution in FIB machining, forcing the use of assumptions. In many cases, the average results measured by experiments will hide the fact of dynamic damage processes in target materials under different irradiation conditions.

On the other hand, molecular dynamic (MD) simulations method constitutes a powerful approach to address some fundamental issues of ion-solid interaction with regard to its capacity in tracking atoms dynamically. Numerous MD simulations have been carried out to study the production of atomic defects in collision cascades [20-22] and the subsequent thermalisation of the disordered particles such as the local melting [23, 24] and the thermal/athermal recrystallization of pre-existing damage [25, 26] over a large variety of materials, probing the areas outside the range of experimental observation. However, the spatial and time scales of many early models were too small to fully track the whole process of multi-particle collision. In recent years, the rapid progress in developing the computer power capacity, particularly the development of cluster parallel computing technique, has largely increased the size of MD computing domain and enabled the promised elucidation of multi-particle

collision processes. Some newly developed three-dimensional models are emerging to address the ion-induced damage and thermal annealing process [27, 28], and the effects of ion fluence [29, 30] and incident angle [31] on the structure and properties of target materials. Large-scale MD computational domain and a combination of ZBL (Ziegler, Biersack and Littmark) and Tersoff potential functions have been reported to help express accurately the stopping of incident ions and the fully track of thermal spike [32, 33].

In this work, the focus will be on the nanocharacterization of FIB-induced damage in a single crystal diamond tool. A series of TEM inspections were carried out to measure the FIB-induced damage layer in the diamond tool under different FIB irradiation conditions. A large-scale multi-particle collision model was developed to emulate the energetic ion collision process and so as to aid the interpretation of the experimental results. This, together with TEM measurements, allowed precisely describing the dynamic amorphisation of diamond. The analysis will be an important guide for any application where a commercial FIB liquid metal ion source (LMIS) system is used in processing or analysing diamond.

2 Experimental setup

In this study, a FEI Nova 200 nanolab dual beam FIB system with Ga ion source was used for both the ion irradiation of a diamond tool and the TEM sample preparation. The ion implantation was carried out normal to the rake face of a diamond tool ((1 0 0) lattice plane) with an irradiation area of 2.0 × 0.5 μm^2. Three acceleration voltages, 8 kV, 16 kV, and 30 kV were used to mill the irradiation area to a same depth of 0.5 μm. The ion fluences are 9.71×10^{20} ions/cm^2, 7.75×10^{20} ions/cm^2, and 7.54×10^{20} ions/cm^2 for the acceleration voltages of 8 kV, 16 kV, and 30 kV, respectively.

The procedure of TEM sample preparation is summarized in figure 1. After the FIB irradiation, the diamond sample was covered with Pt stripes deposited through a standard e-beam deposition process to protect the created damage layer from additional Ga^+ implantation during the following TEM sample preparation procedures. To avoid the charging effect, a thick Pt cover was further deposited on the irradiation area through ion-beam Pt deposition. The cross-sectional TEM sample was prepared using the standard lift-out technique, described in [34]. The final TEM sample is shown in figure 3 (a). The sample was then examined by a FEI Tecnai T20 transmission electron microscopes (TEM)

operated at 200 keV. The convergent beam electron diffraction (CBED) integrated in the TEM system was performed to characterise the crystal structure of the irradiated region.

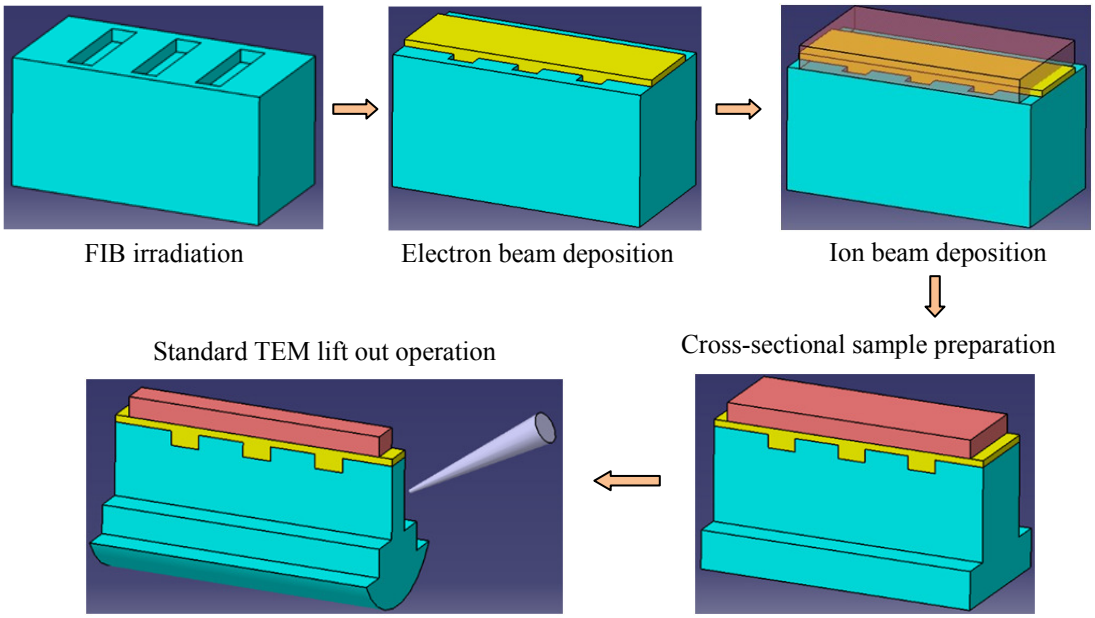

Figure 1: The procedure of FIB irradiation and TEM sample preparation.

3 MD simulation

For the energetic ion collision process, it is important to make sure that the system size is able to track all the stopping processes of incident particles. In this study, the multi-particle collision MD model was built as shown in figure 2. The free boundary condition was used to avoid the reflection effect caused by using fixed or period boundary conditions. The diamond bulk is a square box with dimensions of $50a_1 \times 50a_1 \times 60a_1$, composed of 1,217,161 atoms in total. The lattice constant a_1 is 3.567 Å for single crystal diamond. The three orientations of the workpiece are [1 0 0], [0 1 0] and [0 0 1] in the X, Y and Z directions, respectively (figure 2 (a)). Except the collision surface, all of the rest surfaces were built with a thermal layer with thicknesses of $2a_0$ to control the temperature at 297 K.

A combination of the Tersoff-potential [35] with the ZBL potential [36] was used to describe the interactions between atoms. The Tersoff.ZBL potential function includes a three-body Tersoff potential with a close-separation pairwise modification based on a Coulomb potential and the Ziegler-Biersack-Littmark universal screening function (ZBL potential function), giving the energy E of a system of atoms as:

$$E = \frac{1}{2}\sum_{i}\sum_{j\neq i}((1 - f_F(r_{ij}))V_{ij}^{ZBL} + f_F(r_{ij})V_{ij}^{Tersoff}) \quad (1)$$

$$f_F(r_{ij}) = \frac{1}{1 + e^{-A_F(r_{ij} - r_C)}} \quad (2)$$

where the V_{ij}^{ZBL} and $V_{ij}^{Tersoff}$ indicate ZBL portion and Tersoff portion, respectively. The distance between atoms i and j is r_{ij}. The f_F term is a fermi−like function used to smoothly connect the ZBL repulsive potential with the Tersoff potential. A_F controls how "sharp" the transition is between the two portions, and r_C is essentially the cutoff distance for the ZBL potential.

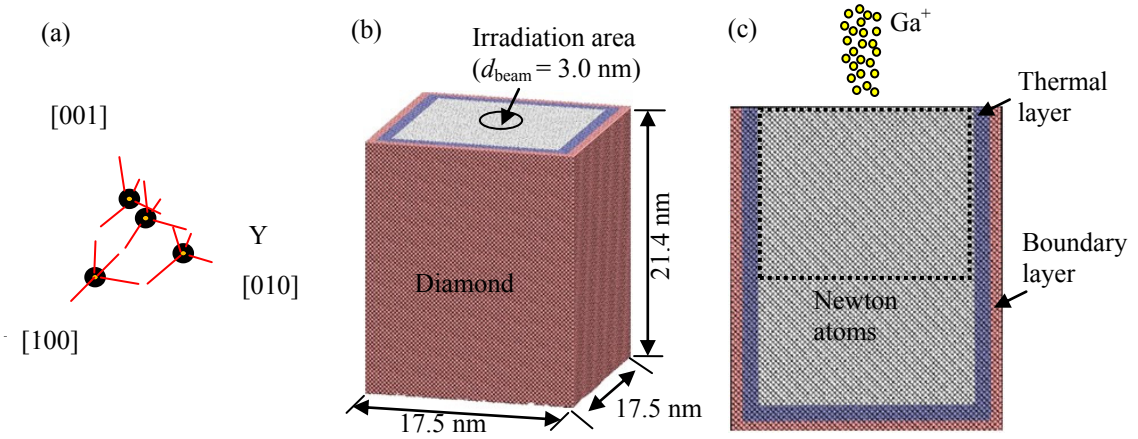

Figure 2: Multi-particle collision MD simulation model. (a) The diamond structure. (b) The dimensions of the diamond bulk model. (c) A cross-sectional view of the workpiece. The dotted line in figure 2 (c) indicates the core collision area selected for temperature analysis.

The MD simulations were implemented through an open source code, LAMMPS [37], complied on a high performance computing (HPC) platform using 32 cores. At the beginning of ion collision, the gallium ions were introduced at a random location above the irradiation area (d_{beam} = 3.0 nm) as shown in figure 2 (c), having no mass, velocity, or potential with any of the C atoms in the system. During the collision process, the particles were then turned on, one by one, having the correct mass of gallium and the velocity corresponding to the energy of beam. After each ion collision, the system was equilibrated via the velocity scaling stochastic layer until a point when the energy of the system has relaxed to a corresponding temperature of 293 K. The next gallium particle was then allowed to impinge onto the sample until the last ion collision finished. Additionally, the concept of atomistic equivalent

temperature [38] was employed to characterise the local thermal spike at the core collision area which has a size of $40a_1 \times 40a_1 \times 35a_1$ (indicated by the dotted line in figure 2 (c)). For the purpose of concision, the simulation parameters are listed in Table 1.

Table 1: MD simulation parameters for ion collsion under 8kV and 16kV.

Simulation parameters	**8kV irradiation**	**16kV irradiation**
Workpiece material	Diamond	Diamond
Workpiece dimensions	$50a_1 \times 50a_1 \times 60a_1$ (a_1 = 3.567 Å)	$50a_1 \times 50a_1 \times 60a_1$ (a_1 = 3.567 Å)
Number of atoms	1,217,184	1,217,184
Sputtered area (d_{beam})	3 nm	3 nm
Incident angle	0º	0º
Interval time	21.5 ps	26.5 ps
Time step	0.1fs	0.1fs
Initial temperature	293K	293K
Ensemble	NVE	NVE

4 Results and discussion

4.1 EFTEM observation of the damage layer

The cross-sectional EFTEM (Energy filtered transmission electron microscopy) images of the damage areas in diamond after the FIB irradiation are shown in figure 3. The FIB sputtered regions under different beam voltages are markedly visible below the deposited Pt cover. Because the electrons will be scattered in arbitrary directions in amorphous materials, the absence of any diffraction contrast in the damage areas indicates that the crystal structures of the damage layers are amorphous (as shown in figures 3 (b)-(d)). The thicknesses of the FIB-induced damage layers in the diamond tool are in a range of tens of nanometres depending on the beam voltage. Moreover, the thickness of ion-induced damage layer increases with the beam energy. The measured thicknesses of the damaged layers were 11.5 nm, 19.4 nm, and 27.6 nm for the beam voltages of 8 kV, 16 kV, and 30 kV, respectively. Moreover,

noticeable dark patches were were found at the interface between the damage layer and the diamond bulk. These dark regions may result from the increase of local density of that area caused by the high concentration of the implanted gallium particles (figures 3 (c) and (d)). Additionally, the dark region observed inside the diamond bulk might be the aggregated form of nitrogen (marked as flaw) which is usually found in natural single crystal diamonds.

In addition, elemental mapping was carried out to determine the relative gallium and carbon distribution in the damaged regions. As shown in figure 4, the visible white areas indicate the distribution of the targeted element. Figures 4 (a)-(c) represent the mapped carbon distributions, and figures 4 (d)-(f) represent the mapped gallium distributions. The results indicate that, under all the tested beam voltage, the implanted Ga ions were concentrated at the damaged region. No visible Ga^+ was found to move deeper into the diamond bulk for the beam voltage applied. Compared with the sharp and narrow Ga signal maps of 16 kV and 30 kV irradiations, a wide fuzzy Ga signal (figure 4-3 (d)) was observed for the 8 kV FIB irradiation. This phenomenon might be linked to the fact that a larger Ga^+ dose is required when sputtering the same volume of diamond materials using a low beam voltage.

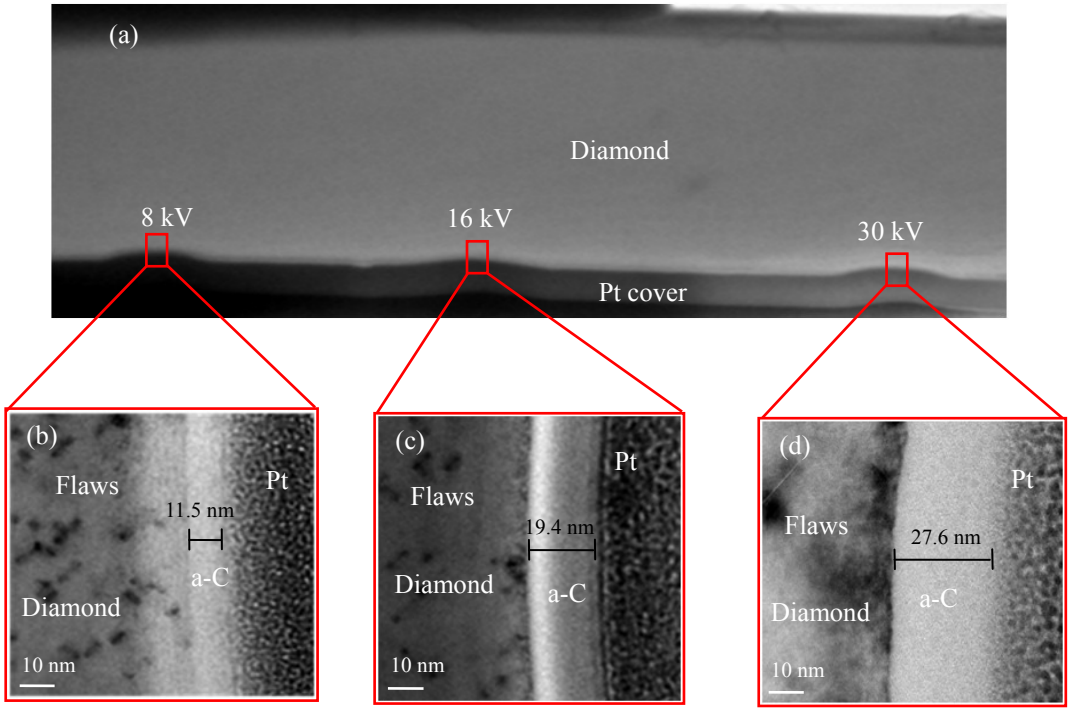

Figure 3: EFTEM images of the ion-induced damage areas. (a) The TEM sample after thinning; (b)-(d) are the EFTEM images showing the ion-induced damage layers formed under beam voltages of 8 kV,

16kV, and 30kV, respectively.

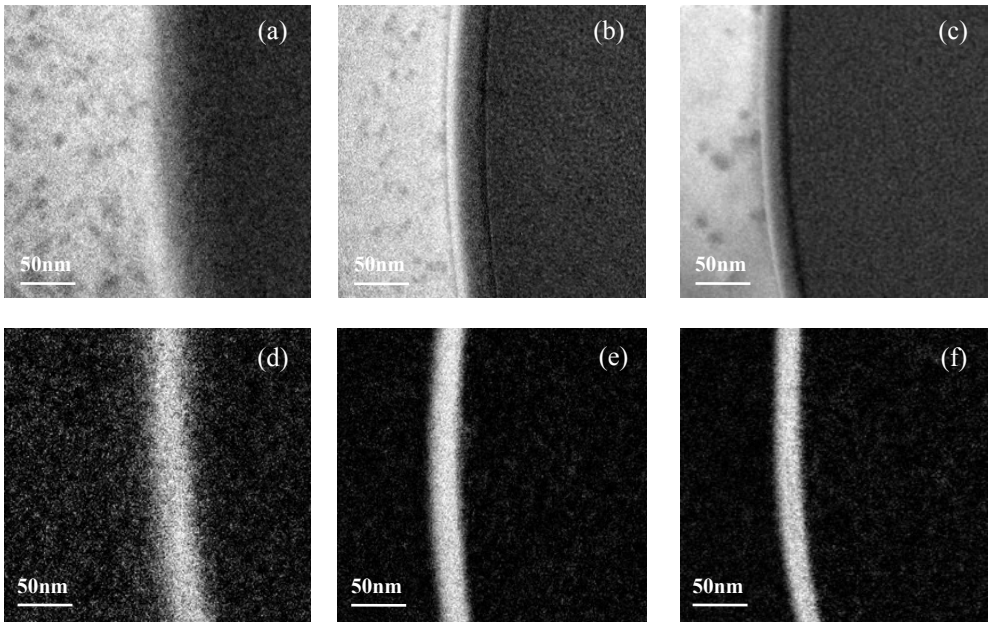

Figure 4: EFTEM images of the mapped element distributions. (a)-(c) represent the mapped carbon distributions; (d)-(f) represent the mapped gallium distributions. (The applied beam voltages are 8 kV (left column), 16 kV (middle column), and 30 kV (right column)).

4.2 Characterization of the damaged region

In order to further characterise the lattice structure of the damaged layer, CBED tests were carried out with the electron beam focusing onto the centre of damaged regions (figure 5 (a)). The diameter of the spot is around 20 nm. For reference, the CBED patterns of the single crystal diamond bulk and the deposited Pt cover were measured and shown in figures 5 (b)-(c).

Figures 5 (d)-(f) list the CBED patterns of the damage layers created under beam voltages of 8 kV, 16 kV, and 30 kV, respectively. It is found that the damage layer created under 8 kV has high proportion of diamond structure. However, for the 16 kV and 30 kV irradiations, the diamond signals in the CBED patterns were remarkably weaker. The muzzy of the diamond signal in the CBED patterns proves that the irradiation has created large amount of non-diamond clusters in the diamond matrix. Thus, the irradiation of the diamond tool at an increasing beam voltage results in an increase of the level of amorphization of diamond. The increase of non-diamond phase with the beam voltage is associated with the growth of the number of sp^2 bonded C atoms and local thermal recrystallization

during each ion collision process, which will be discussed in next section.

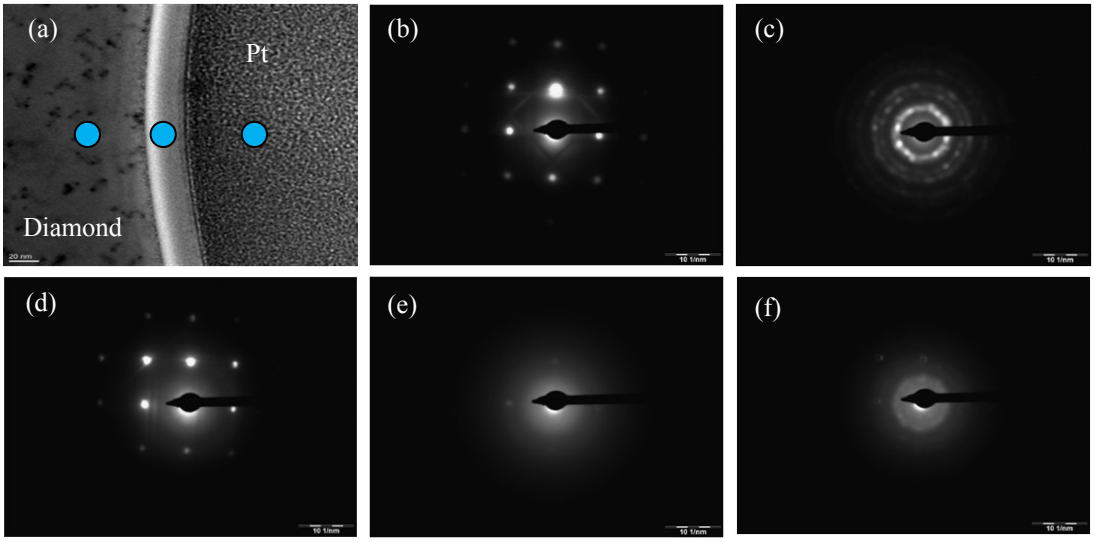

Figure 5: CBED analysis of the damage regions under different FIB irradiation voltages. (a) A zero-energy-loss TEM image of FIB irradiated area with the blue spots to schematically indicate the electron beam focusing point when carrying out the CBED tests; (b) CBED pattern of diamond bulk; (c) CBED pattern of Pt cover; (d)-(f) CBED patterns of damage layers created under beam voltages of 8 kV, 16 kV, and 30 kV, respectively.

4.3 Dynamic ion damage in FIB milling

4.3.1 The damage layer predicted by multi-particle collision

In a typical LMIS based Ga^+ FIB beam milling process, the energy transferred by the incident Ga^+ is usually sufficient to break the C-C bond leading to the displacement of lattice atoms, formation of point defects, surface sputtering and the production of other secondary processes. It is assumed that when the density of point defect is sufficient high, the displaced atoms would partly re-order into different characteristic arrangements of atoms and a residual damage layer is formed at the near surface comprised mostly of vacancies and interstitials. In this study, the ion-solid interactions physics leading to processing defects in FIB machining were emulated by MD simulations.

Figures 6 and 7 compare the inside views of the atomic defects formed in diamond bulk under 8 keV and 16 keV Ga^+ impacts, respectively. Each diamond atom was coloured by the atom's common

neighbour analysis (CNA) value. The cyan atoms represent the two-fold coordinated C atoms and the purple atoms represent three-fold coordinated C atoms (sp^2 hybridization). The defect-free regions (sp^3 hybridization) were removed from the visualizations. It is found that the thickness of the residual damage layer for 8 keV impact is about 14.5 nm, while a larger value of 19.6 nm was found for the 16 keV impact. Compared with the 8 keV multi-particle collision, an apparent larger volume of damaged region was formed by the 16 keV collision. The diameters of the core damaged regions are 6.0 nm and 7.2 nm for 8 keV and 16 keV collisions, respectively.

Moreover, the maximum depths of the implanted gallium ions (yellow colour) are 10.5 nm and 12.8 nm for 8 keV and 16 keV impacts, respectively (figure 6 (c) and figure 7 (c)). The implanted gallium particles tend to distribute in the amorphous carbon layer (marked as a-C) towards the interface of a-C and diamond bulk. As a result, the local density of the interface of a-C and diamond bulk is slightly larger than the upper surface. This phenomenon agreed well with the dark patches located at the interface between a-C layer and the diamond bulk observed in the EFTEM images (figures 3 (c) and (d)).

In addition, the radial distribution functions (RDF), g(r), of the damaged zones created during the collisions were calculated and shown in figure 8. Ideally, for a diamond crystal, g(r) is centred at diamond bond length (1.54 Å) for the shortest range order. After the collision, the peak values of g(r) within a single lattice were reduced and the peak at the shortest distance (1.54 Å) becomes apparently broader, signifying the characteristic to the g(r) of amorphous structure. The peak value of g(r) was found to be decreased with the increase of the energy incident particles, indicating that high energetic collision can create high disordered clusters in the diamond matrix.

Therefore, the MD simulation results compare closely with the corresponding data derived from experiments as discussed above. The nature of FIB-induced damaged layer in the diamond tool is a mixture phase of sp^2 and sp^3 hybridization and accommodates a significant proportion of the implanted gallium. The range of the damaged layer significantly depends on the beam voltage applied.

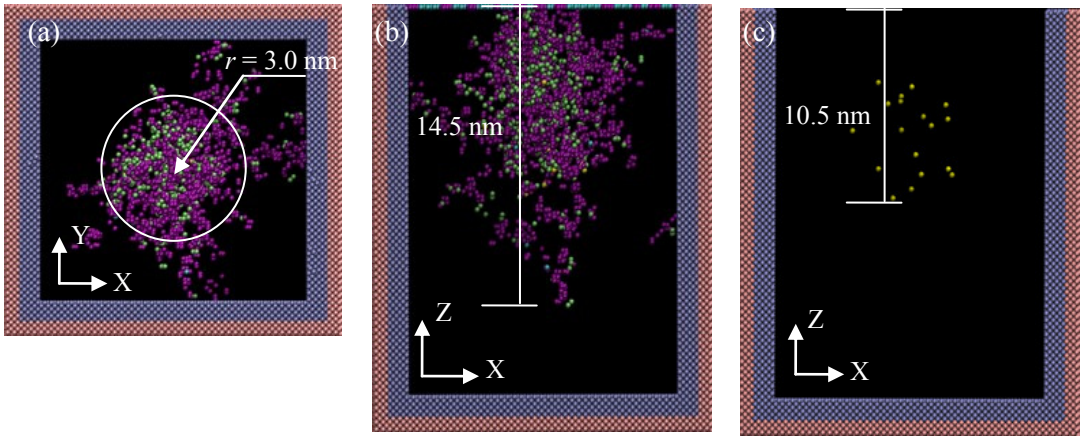

Figure 6: The internal images of the damaged area after 8 keV Ga^+ implantation with a fluence of 3.0 × 10^{14} ions/cm^2. (a) Plan view of amorphous region; (b) cross-sectional view of amorphous region; and (c) the distribution of the implanted gallium particles. The cyan atoms represent the 2-fold coordinated C atoms and purple atoms represent 3-fold coordinated C atoms. The yellow atoms represent the implanted gallium particles.

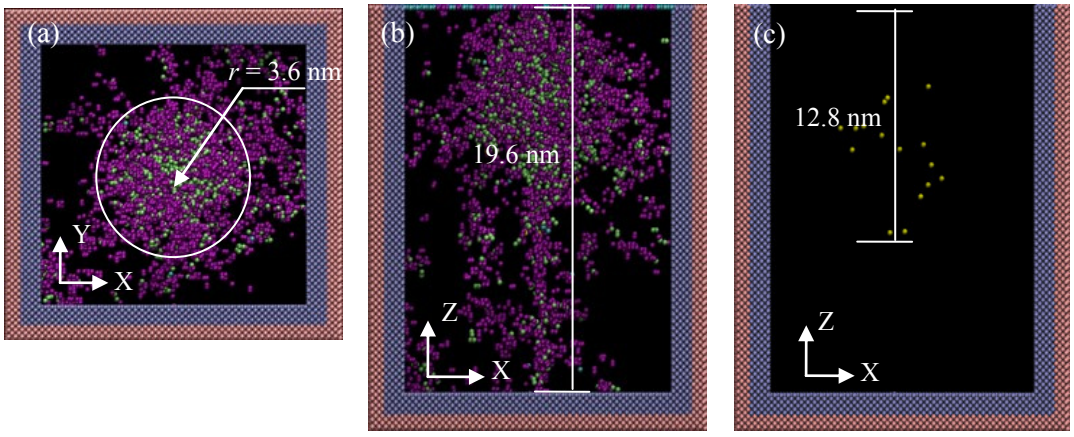

Figure 7: The internal images of the damaged area after 16 keV Ga^+ implantation with a fluence of 3.0 × 10^{14} ions/cm^2. (a) Plan view of amorphous region; (b) cross-sectional view of amorphous region; and (c) the distribution of the implanted gallium particles. The cyan atoms represent the 2-fold coordinated C atoms and purple atoms represent 3-fold coordinated C atoms. The yellow atoms represent the implanted gallium particles.

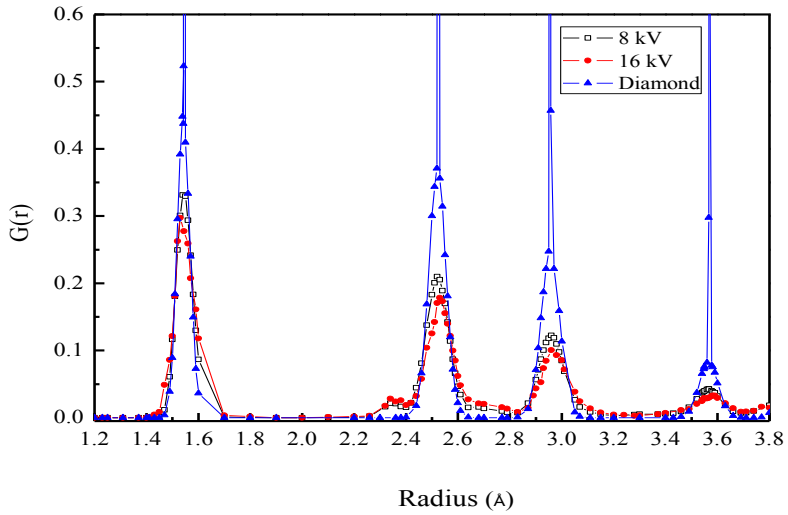

Figure 8: The RDF distribution of irradiation area under different beam voltages.

4.3.2 Dynamic damage process under different beam voltages

Figure 9 shows the local temperature evolution of the first ion collision. As compared with the 8 keV collision, a higher peak value of the local temperature (1454.6 K) and a longer life time of the local high temperature spike (above 800 K) were observed for the 16 keV collision. This difference enabled the incident Ga particle with a higher impulse to move deeper into the diamond bulk, and thus generated a thicker atomic defects layer after multi-particle collision. Moreover, the high local temperature at the very core collision area would soften the C-C bond strength of diamond and provide the necessary thermal energy required by the local recrystallization of the atomic defects. As an example shown in figure 10, the variations of the number of atomic defects for the first ion collision were compared between the low energy (8 keV) and the high energy (16 keV) collisions. It is found that the number of atomic defects reaches a peak value and then partly re-crystallises back to diamond structure. Nevertheless, more atomic defects are created under the 16 keV Ga^+ impact. The recrystallization process completed within 0.8 ps, and the numbers of the residual defects are 271 and 416 for 8 keV and 16 keV collisions, respectively.

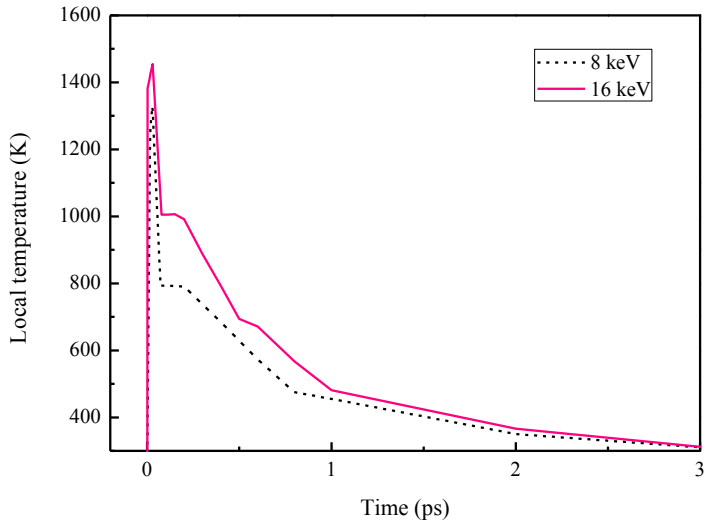

Figure 9: The evolution of local temperature for the first ion collision.

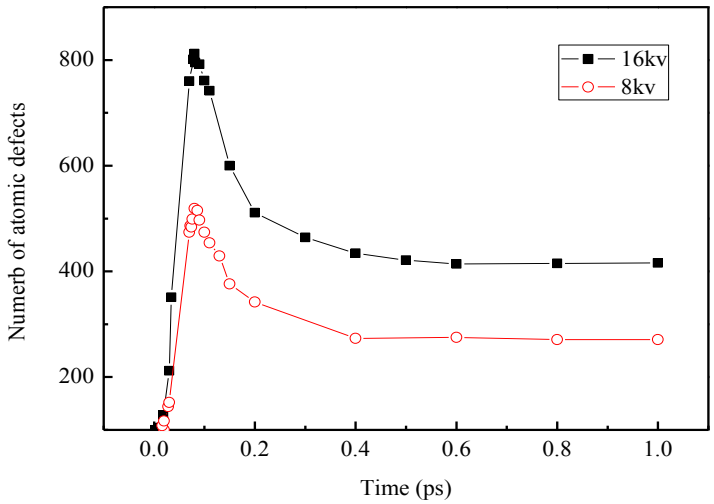

Figure 10: The variation of the number of defects during the first ion collision.

Moreover, with the increase of ion dose, the residual defects created inside the diamond matrix undergo an accumulation process. The yields of residual atomic defects per ion were summarized in figure 11. It is found that the increment of atomic defects gradually decreases with the increase of ion dose. This might be due to the fact that the atomic defects created by the former ion collision will be partly annealed during the subsequent ion collision process. Figure 12 summarise the variation of the number of atomic defects with the increase of ion fluence. It is found that the number of atomic defects is essentially linear up to a special ion fluence of 2.0×10^{14} ions/cm^2; above this ion fluence the curve gradually tends to approach a stable value which depends on the kinetic energy of the

incident ion.

Indeed, there exists two competitive processes in a typical FIB machining—damage formation and sputtering, and the FIB sputtering occurs in the created damage layer with further damage formation [18]. With the increase of the ion fluence, the number of defects and the density of the non-diamond phase's layer increased [17]. The saturation of the non-diamond phase would suppress the formation of new atomic defects. Additionally, the formation of atomic defects would also result in the alternation of the local physical and chemical properties of diamond, and a change in the ion sputter yield. It is therefore anticipated that after reaching a critical ion dose, at which the increased material removal rate reaches the damage formation rate, a stabilization of the a-C layer is likely to be obtained.

Most recently, few attempts have been made to study the ion-induced amorphisation of diamond. In a test of 30 keV Ga^+ irradiation of synthetic type1b diamond substrate, an amorphous damage layer of 44 nm was formed when the ion dose delivered to the sample exceeds a critical amorphisation dose [18]. Similarly, an amorphous damage layer of 35 nm was reported in 30 keV Ga^+ irradiation of CVD diamond [19]. In this study, the thickness of the equilibrium damage layer formed at the surface of the single crystal diamond tool was found to increase with the beam voltage, and the maximum thickness of the damaged layer is 27.6 nm under 30 kV FIB irradiation. These, together with the MD simulations, further identify the impulse-dependent amorphization of the diamond. The thickness and the amorphization level of the equilibrium damage layer depend significantly on the beam voltage.

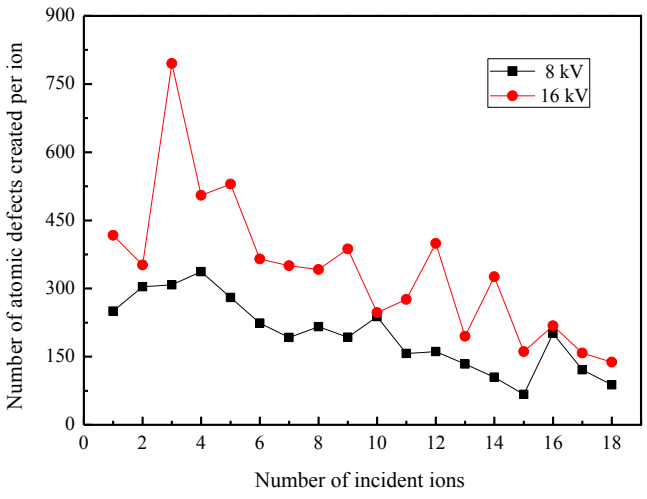

Figure 11: The yield of the three-fold coordinated atoms for each ion collision.

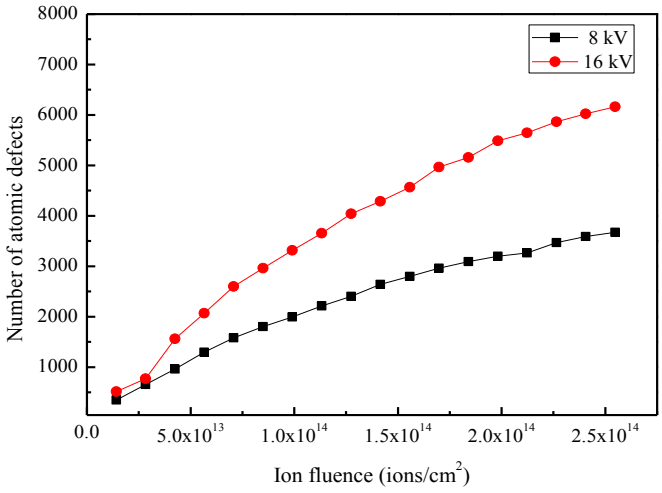

Figure 12: The variation of the number of the atomic defects with the ion fluence.

4.4 Suggestions for FIB based tool fabrication process

Currently, the FIB-induced residual damage on micro- and nanoscale diamond tools and its effects on the performance of the cutting tools have received increasing interest. In our previous research on the nanometric cutting of nanostructures using a nanoscale multi-tip diamond tool fabricated by FIB, the tool wear was found on both the clearance face and the sides of the tool tips after a cutting distance of 2.5 km [13]. Apart from the compress stress produced at the sides of the tool tips, the research findings from this work indicate that the ion irradiation induced doping and defects are also responsible for the initiation of tool wear.

In both of the TEM experiments and the MD simulations, the thickness and the amorphization level of the FIB-induced damage layer significantly increase with the beam voltage. As a consequence of the large difference in bond strength between the sp^3 hybridization and the sp^2 hybridization, the macroscopic and microscopic properties of the amorphous carbon layer are quite different from the diamond bulk. As schematically shown in figure 13, upon nanometric cutting, the damage layer will worn away firstly because of its non-diamond phase. Most recently, similar phenomenon has been reported in micro machining of NiP using a FIB-irradiated single tip diamond tool [39, 40].

Therefore, the FIB-induced damage layer should be paid enough attention when shaping the cutting edges of diamond tools. It will become more important when the dimensions of a multi-tip diamond

tool are approaching its ultimate values. The investigation of amorphization of diamond indicate that decreasing the FIB processing energy can effectively reduce the Ga^+ implantation depth as well as the thickness of a-C layer, and it is thus recommended when tailing the diamond tool tip.

Nevertheless, since the maximum thickness of the damage layer of FIB irradiated diamond is about 27.6 nm, which is 1 part in 10^4 of the functional dimension of a micro cutting tool, the ion induced damage might be neglected for micro scale applications.

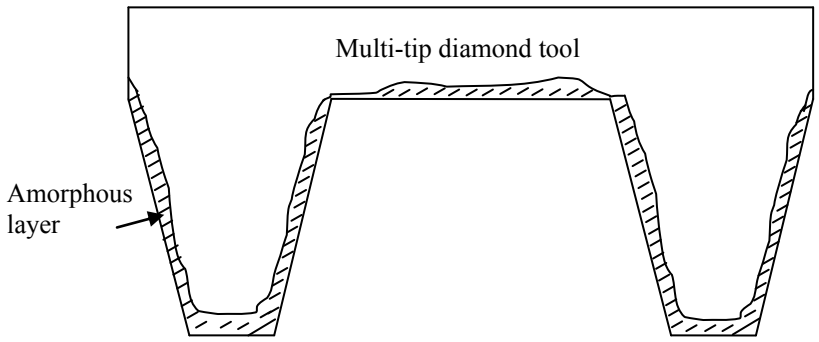

Figure 13: Schematically show of the early tool wear region of a multi-tip diamond tool by considering FIB-induced damage layer.

5 Conclusions

In this work, TEM experiments and MD simulations have been carried out to characterise the feature of FIB-induced damage in a single crystal diamond tool under different beam voltages. The results obtained from experiments and simulations have good agreement. In both the TEM measurements and the MD simulations, the FIB irradiation will create a surface damage layer (a mixture phase of sp^2 and sp^3 hybridization and accommodates a significant proportion of the implanted gallium) in diamond. For the tested beam voltages in a typical FIB system, the thicknesses of the damaged layers formed on a diamond tool surface increased from 11.5 nm to 27.6 nm.

The dynamic creation of atomic defects leading to the amorphization of diamond has also been emulated by the MD simulations. The formation of atomic defects, the thermal spike and the recrystallization of atomic defects have been observed during each single ion collision process. The thickness and the amorphization level of the equilibrium damage layer depend significantly on the beam voltage. Moreover, the research findings of this research work predict that the non-diamond

phase of residual damage layer around tool tips will wear first during nanometric cutting. Low-energy FIB polishing is recommended when tailing the diamond tool tip by FIB.

Acknowledgements

The authors gratefully acknowledge the financial support from EPSRC (EP/K018345/1). The authors would also like to acknowledge the technical supports from the Kelvin Nanocharacterisation Centre of the University of Glasgow for assistance with FIB and TEM measurements.

Reference

[1] X. Luo, K. Cheng, D. Webb, and F. Wardle, "Design of ultraprecision machine tools with applications to manufacture of miniature and micro components," *Journal of Materials Processing Technology,* vol. 167, pp. 515-528, 2005.

[2] E. Brinksmeier, R. Gläbe, and L. Schönemann, "Diamond Micro Chiseling of large-scale retroreflective arrays," *Precision Engineering,* vol. 36, pp. 650-657, 2012.

[3] J. Yan, K. Maekawa, J. i. Tamaki, and T. Kuriyagawa, "Micro grooving on single-crystal germanium for infrared Fresnel lenses," *Journal of micromechanics and microengineering,* vol. 15, p. 1925, 2005.

[4] F. Fang and Y. Liu, "On minimum exit-burr in micro cutting," *Journal of Micromechanics and Microengineering,* vol. 14, p. 984, 2004.

[5] J. Sun, X. Luo, W. Chang, J. Ritchie, J. Chien, and A. Lee, "Fabrication of periodic nanostructures by single-point diamond turning with focused ion beam built tool tips," *Journal of Micromechanics and Microengineering,* vol. 22, p. 115014, 2012.

[6] X. Ding, A. Jarfors, G. Lim, K. Shaw, Y. Liu, and L. Tang, "A study of the cutting performance of poly-crystalline oxygen free copper with single crystalline diamond micro-tools," *Precision engineering,* vol. 36, pp. 141-152, 2012.

[7] Z. Xu, F. Fang, S. Zhang, X. Zhang, X. Hu, Y. Fu*, et al.*, "Fabrication of micro DOE using micro tools shaped with focused ion beam," *Optics express,* vol. 18, pp. 8025-8032, 2010.

[8] M. J. Vasile, R. Nassar, J. Xie, and H. Guo, "Microfabrication techniques using focused ion beams and emergent applications," *Micron,* vol. 30, pp. 235-244, 1999.

[9] D. Adams, M. Vasile, T. Mayer, and V. Hodges, "Focused ion beam milling of diamond: effects of H 2 O on yield, surface morphology and microstructure," *Journal of Vacuum Science & Technology B: Microelectronics and Nanometer Structures,* vol. 21, pp. 2334-2343, 2003.

[10] Y. N. Picard, D. Adams, M. Vasile, and M. Ritchey, "Focused ion beam-shaped microtools for ultra-precision machining of cylindrical components," *Precision Engineering,* vol. 27, pp. 59-69, Jan 2003.

[11] X. Ding, G. Lim, C. Cheng, D. L. Butler, K. Shaw, K. Liu*, et al.*, "Fabrication of a micro-size diamond tool using a focused ion beam," *Journal of Micromechanics and Microengineering,* vol. 18, p. 075017, 2008.

[12] Z. Tong, Y. Liang, X. Jiang, and X. Luo, "An atomistic investigation on the mechanism of machining nanostructures when using single tip and multi-tip diamond tools," *Applied Surface Science,* vol. 290, pp. 458-465, 2014.

[13] X. Luo, Z. Tong, and Y. Liang, "Investigation of the shape transferability of nanoscale multi-tip diamond tools in the diamond turning of nanostructures," *Applied Surface Science,* vol. 321, pp. 495-502, 2014.

[14] J. Sun and X. Luo, *Deterministic Fabrication of Micro-and Nanostructures by Focused Ion Beam*: Springer, 2013.

[15] D. D. Cheam, K. A. Walczak, M. Archaya, C. R. Friedrich, and P. L. Bergstrom, "Leakage current in single electron device due to implanted gallium dopants by focus ion beam," *Microelectronic Engineering,* vol. 88, pp. 1906-1909, 2011.

[16] H. Gnaser, B. Reuscher, and A. Brodyanski, "Focused ion beam implantation of Ga in nanocrystalline diamond: Fluence-dependent retention and sputtering," *Nuclear Instruments and Methods in Physics Research Section B: Beam Interactions with Materials and Atoms,* vol. 266, pp. 1666-1670, 2008.

[17] R. Brunetto, G. A. Baratta, and G. Strazzulla, "Amorphization of diamond by ion irradiation: a Raman study," in *Journal of Physics: Conference Series*, 2005, p. 120.

[18] S. Rubanov and A. Suvorova, "Ion implantation in diamond using 30keV Ga+ focused ion beam," *Diamond and Related Materials,* vol. 20, pp. 1160-1164, 2011.

[19] W. McKenzie, M. Z. Quadir, M. Gass, and P. Munroe, "Focused ion beam implantation of diamond," *Diamond and Related Materials,* vol. 20, pp. 1125-1128, 2011.

[20] R. Averback, "Atomic displacement processes in irradiated metals," *Journal of nuclear materials,* vol. 216, pp. 49-62, 1994.

[21] D. Bacon, A. Calder, F. Gao, V. Kapinos, and S. Wooding, "Computer simulation of defect production by displacement cascades in metals," *Nuclear Instruments and Methods in Physics Research Section B: Beam Interactions with Materials and Atoms,* vol. 102, pp. 37-46, 1995.

[22] M. Caturla, T. Diaz de la Rubia, and G. H. Gilmer, "Disordering and defect production in silicon by keV ion irradiation studied by molecular dynamics," *Nuclear Instruments and Methods in Physics Research Section B: Beam Interactions with Materials and Atoms,* vol. 106, pp. 1-8, 1995.

[23] H. Gades and H. M. Urbassek, "Dimer emission in alloy sputtering and the concept of the “clustering probability”," *Nuclear Instruments and Methods in Physics Research Section B: Beam Interactions with Materials and Atoms,* vol. 103, pp. 131-138, 1995.

[24] W. Phythian, R. Stoller, A. Foreman, A. Calder, and D. Bacon, "A comparison of displacement cascades in copper and iron by molecular dynamics and its application to microstructural evolution," *Journal of Nuclear Materials,* vol. 223, pp. 245-261, 1995.

[25] J. Nord, K. Nordlund, and J. Keinonen, "Amorphization mechanism and defect structures in ion-beam-amorphized Si, Ge, and GaAs," *Physical Review B,* vol. 65, p. 165329, 2002.

[26] K. Nordlund and R. Averback, "Point defect movement and annealing in collision cascades," *Physical Review B,* vol. 56, p. 2421, 1997.

[27] D. Saada, J. Adler, and R. Kalish, "Transformation of Diamond (sp3) to Graphite (sp2) Bonds by Ion-Impact," *International Journal of Modern Physics C,* vol. 9, pp. 61-69, 1998.

[28] D. Saada, J. Adler, and R. Kalish, "Computer simulation of damage in diamond due to ion impact and its annealing," *Physical Review B,* vol. 59, p. 6650, 1999.

[29] S.-i. Satake, S. Momota, S. Yamashina, M. Shibahara, and J. Taniguchi, "Surface deformation of Ar+ ion collision process via molecular dynamics simulation with comparison to experiment," *Journal of Applied Physics,* vol. 106, p. 044910, 2009.

[30] S.-i. Satake, S. Momota, A. Fukushige, S. Yamashina, M. Shibahara, and J. Taniguchi, "Molecular

dynamics simulation of surface deformation via Ar+ ion collision process," *Nuclear Instruments and Methods in Physics Research Section B: Beam Interactions with Materials and Atoms,* vol. 272, pp. 5-8, 2012.

[31] X. Li, P. Ke, K.-R. Lee, and A. Wang, "Molecular dynamics simulation for the influence of incident angles of energetic carbon atoms on the structure and properties of diamond-like carbon films," *Thin Solid Films,* vol. 552, pp. 136-140, 2014.

[32] R. Smith, S. D. Kenny, and D. Ramasawmy, "Molecular-dynamics simulations of sputtering," *Philosophical Transactions of the Royal Society of London. Series A: Mathematical, Physical and Engineering Sciences,* vol. 362, pp. 157-176, 2004.

[33] S.-i. Satake, N. Inoue, J. Taniguchi, and M. Shibahara, "Molecular dynamics simulation for focused ion beam processing: a comparison between computational domain and potential energy," in *Journal of Physics: Conference Series*, 2008, p. 012013.

[34] D. Hickey, E. Kuryliw, K. Siebein, K. Jones, R. Chodelka, and R. Elliman, "Cross-sectional transmission electron microscopy method and studies of implant damage in single crystal diamond," *Journal of Vacuum Science & Technology A,* vol. 24, pp. 1302-1307, 2006.

[35] J. Tersoff, "Modeling solid-state chemistry: Interatomic potentials for multicomponent systems," *Physical Review B,* vol. 39, p. 5566, 1989.

[36] J. F. Ziegler and J. P. Biersack, "The stopping and range of ions in matter," in *Treatise on Heavy-Ion Science*, ed: Springer, 1985, pp. 93-129.

[37] S. Plimpton, "Fast parallel algorithms for short-range molecular dynamics," *Journal of computational physics,* vol. 117, pp. 1-19, 1995.

[38] Z. Tong, Y. Liang, X. Yang, and X. Luo, "Investigation on the thermal effects during nanometric cutting process while using nanoscale diamond tools," *The International Journal of Advanced Manufacturing Technology,* pp. 1-10, 2014.

[39] N. Kawasegi, K. Ozaki, N. Morita, K. Nishimura, and H. Sasaoka, "Single-crystal diamond tools formed using a focused ion beam: Tool life enhancement via heat treatment," *Diamond and Related Materials,* vol. 49, pp. 14-18, 2014.

[40] N. Kawasegi, T. Niwata, N. Morita, K. Nishimura, and H. Sasaoka, "Improving machining performance of single-crystal diamond tools irradiated by a focused ion beam," *Precision Engineering,* vol. 38, pp. 174-182, 2014.